


Removal of erythrosine B dye from wastewater using chitosan boric acid composite material: Experimental and density functional theory findings

Hüseyin Fatih Çetinkaya¹ | Meltem Sarioğlu Cebeci¹ | Savaş Kaya²  |
Nida Shams Jalbani³ | Mikhail M. Maslov⁴ | Riadh Marzouki^{5,6}

¹Department of Environmental Engineering, Faculty of Engineering, Sivas Cumhuriyet University, Sivas, Turkey

²Department of Pharmacy, Health Services Vocational School, Sivas Cumhuriyet University, Sivas, Turkey

³National Center of Excellence in Analytical Chemistry, University of Sindh, Jamshoro, Pakistan

⁴Department of Condensed Matter Physics, National Research Nuclear University "MEPhI", Moscow, Russian Federation

⁵Chemistry Department, College of Science, King Khalid University, Abha, Saudi Arabia

⁶Chemistry Department, Faculty of Sciences of Sfax, University of Sfax, Sfax, Tunisia

Correspondence

Savaş Kaya, Department of Pharmacy, Health Services Vocational School, Sivas Cumhuriyet University, 58140 Sivas, Turkey.

Email: savaskaya@cumhuriyet.edu.tr

Abstract

In this study, the chitosan boric acid (**Ch-B**) composite has been prepared and characterized with sophisticated analytical techniques such as FT-IR, SEM, and EDX. The prepared **Ch-B** adsorbent was applied for the adsorption of erythrosine B (**EB**) dye from water samples under the optimized parameters of pH, adsorbent dosage, time, and temperature. Results shows that the **Ch-B** adsorbent removes 96.5% of **EB** dye at pH 5, using 0.05 g of adsorbent. The adsorption equilibrium data have been subject to the Langmuir, Freundlich, and D-R adsorption equilibrium models, which demonstrates that the Freundlich model was the best fit with good correlation coefficient value ($R^2 = 0.991$), while energy E ($9.18 \text{ KJ}\cdot\text{mol}^{-1}$) calculated from D-R model suggested that the physical adsorption nature of the adsorption. Beside this, the thermodynamic and kinetic experiments were performed to check the feasibility and adsorption mechanism of EB-dye onto Ch-B adsorbent, which shows that the adsorption is endothermic ($\Delta H = 0.124$) and spontaneous in nature due to the negative values of Gibbs free energy (i.e., $\Delta G \text{ KJ}\cdot\text{mol}^{-1} = -13.01, -17.06, \text{ and } -17.60$). The kinetic models show that the adsorption equilibrium is best fitted with pseudo second order kinetic model due to good correlation coefficient ($R^2 = 0.99$). Moreover, the interaction phenomenon between adsorbent and adsorbate was analyzed through DFT calculations.

KEYWORDS

adsorption, boric acid, chitosan, composite, DFT, erythrosine B

1 | INTRODUCTION

Dyeing industries produce large bodies of wastewater, causing detrimental environmental consequences, and in the elimination of such a gigantic problem, cleaning strategies have adopted various means.^[1] In many of the applications, low-cost adsorbents have been preferred, and a large range of these have already been employed.

Activated carbon, for example, has become prominent owing to its highly selective adsorption capacity. In time, reusability of this adsorbent did not seem to be feasible, and today, naturally occurring adsorbents, such as chitosan and its derivatives, have subsided the interest on active carbon compounds.^[2]

Chitosan (Ch) is the most widely used biological molecule in the adsorption of various water pollutants due to

its many outstanding properties such as biodegradability, biocompatibility, and its high adsorption capacity. These advantageous features can be attributed to the plentitude of amine and hydroxyl functional groups.^[3–5] These groups are versatile in removing contaminants of differing nature by forming electrostatic interactions, hydrogen or chemical bonds.^[6–10] This biopolymer on its own is not refractory to acidic environments, and this negative aspect could be overcome by using it in composite forms.^[11] Many of the approaches have generated chitosan composites by crosslinking,^[12] grafting,^[13] and coupling reactions.^[14] Crosslinking has seemed to be the most suitable way to improve both the physical and chemical properties of Ch, such as physical robustness, and stability in acidic environments.^[15–17] And epichlorohydrin (ECH) (chloromethyl oxirane, C₃H₅ClO) has been the widely used cross-linker.^[18,19]

There have been a number of studies on the dye removal with chitosan composites in the literature. To illustrate, Ch/bentonite (BT) composite, cross-linked with glutaraldehyde, has been tried in the adsorption of an azo dye, amido black 10B.^[20] In another study, a TLAC (titanium and lanthanum oxides impregnated on granular activated carbon)/chitosan composite was synthesized and tested in cleaning wastewater contaminated with crystal violet.^[21]

This study constituted the first attempt to investigate the removal of erythrosine B (EB) dye with a chitosan–boric acid composite. Adsorption kinetics indicated that this new composite was highly effective in the removal of EB from aqueous environments. Physical and chemical parameters of adsorption were determined, and density functional theory (DFT) was employed to better understand the mechanism of adsorption.

2 | EXPERIMENTAL SECTION

2.1 | Materials and methods

All the chemicals used in experiments were analytical grade and used without further purification. The erythrosine B dye (Figure 1) was procured from Sigma–Aldrich while the boric acid, epichlorohydrin (ECH), ethanol (EtOH), hydrochloric acid (HCl), chitosan, sodium hydroxide (NaOH), and sodium tripolyphosphate (NaTPP) were obtained from Merck Company Pvt Ltd. The prepared adsorbent has been characterized by CUTAM Central Laboratory facilities (Sivas Cumhuriyet University, Turkey) using Fourier transform infrared (FTIR) spectrometer (ATR, Bruker, Tensor II), scanning electron microscopy (SEM), and energy dispersive X-ray (EDX) spectroscopy (TESCAN MIRA3 XMU), and

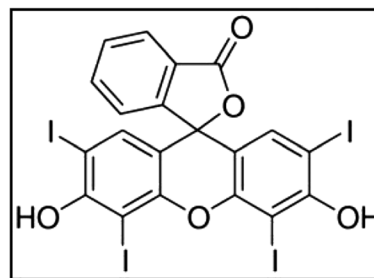


FIGURE 1 Chemical structure of erythrosine B dye

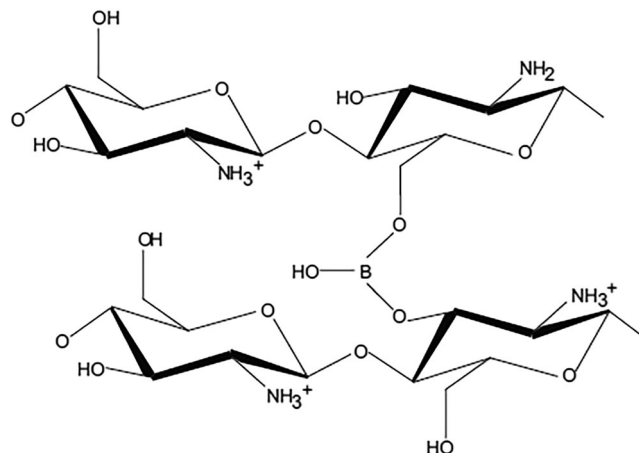


FIGURE 2 Structure of chitosan–boric acid composite

ultraviolet-visible (UV-Vis) spectrometry was used (T-60, China).

2.2 | Preparation of the chitosan–boric acid (Ch-B) composite beads

Double cross-linked chitosan–boric acid composite was formed in spherical entities by using 4 g of chitosan and 4 g boric acid at room temperature (25°C) in 160 ml (5% v/v) acetic acid (Figure 2). The reaction was performed for 3 h, in 160 ml (0.01 M) ECH, pH 10.0. The mixture was added drop wise to 50 mM NaTPP solution and stirred for 3 h at 100 rpm. The beads were then washed and dried at 37°C.^[22]

2.3 | Batch adsorption experiments

The adsorption of EB dye on Ch-B composite was investigated in batch adsorption experiments. Erythrosine B, supplied in analytical purity, was used directly; 1000 mg L⁻¹ EB stock solution was prepared by dissolving the dye.

The stock solution of EB was diluted with deionized water. Adsorption was carried out for 24 h at 25°C in a 10 ml reaction volume, containing 50 mg Ch-B and 100 mg L⁻¹ EB. A pH range from 5.0 to 8.0 was used. Free EB concentration was periodically monitored at 525 nm in a UV-visible using spectrophotometer. Adsorption %, Q (mol·g⁻¹), and % desorption equations were calculated using Equations (1)–(3) below:

$$\text{Adsorption}\% = \left[\frac{C_i - C_f}{C_i} \right] \times 100 \quad (1)$$

$$Q = \left[\frac{C_i - C_f}{C_i} \right] \times V \quad (2)$$

$$\text{Desorption}\% = \left[\frac{Q_{des}}{Q_{ads}} \right] \times 100 \quad (3)$$

where C_i is the initial concentration (mol·L⁻¹); m is the adsorbent mass (g); C_f is the equilibrium concentration (mol·L⁻¹); V is the solution volume (L); Q_{des} is the desorbed amount of erythrosine B (mol·g⁻¹), and Q_{ads} is the adsorbed amount of erythrosine B (mol·g⁻¹).

2.4 | Details of density functional theory calculations

All calculations were performed using the B3LYP exchange-correlation functional^[23,24] and 6-311G (d,p) electronic basis set.^[25] We used the graphics processor-based TeraChem software.^[26–29] Geometry optimization was carried out with the efficient geomeTRIC energy minimizer.^[30] The dispersion corrections D3 proposed by Grimme^[31] were also included to take into account the non-covalent interactions. Conceptual density functional theory (CDFT) presents the following equations to calculate the important quantum chemical parameters like chemical potential (μ), electronegativity (χ), hardness (η), and softness (σ)^[32,33]

$$\mu = -\chi = \left[\frac{\partial E}{\partial N} \right]_{\nu(r)} = -\left(\frac{I+A}{2} \right) \quad (4)$$

$$\eta = \left[\frac{\partial^2 E}{\partial N^2} \right]_{\nu(r)} = I - A \quad (5)$$

$$\sigma = 1/\eta \quad (6)$$

To predict the electrophilicity (ω) of the chemical systems, Parr, Szentpaly, and Liu derived an equation based on the absolute electronegativity and absolute hardness. The derived electrophilicity equation is given as^[32]

$$\omega = \chi^2 / 2\eta \quad (7)$$

In these equations, E , N , I , and A are total electronic energy, total number of the electrons of chemical system, ground state ionization energy, and ground state electron affinity, respectively. Koopmans Theorem^[34] can be considered as a tool to predict the ground state ionization energy and electron affinity of a chemical system. According to the theory, we can write the relations as: $I = -E_{HOMO}$ and $A = -E_{LUMO}$. In the relations given, E_{HOMO} and E_{LUMO} are the energy levels of HOMO and LUMO orbitals, respectively.

3 | RESULTS AND DISCUSSION

3.1 | Characterization

3.1.1 | FT-IR characterization

The Ch-B composite has been characterized by FT-IR spectroscopic techniques (Figure 3). In Figure 3, the spectrum of Ch-B has characteristic peaks at 3236, 2935, 1720, and 1383 cm⁻¹ for OH, C–H, C–O, and C–N stretching frequencies, respectively, while the peak at 1052 cm⁻¹ is due to OH bending. Moreover, the spectrum of loaded EB dye shows absence of some peaks such as 2935, 1720, 1383, and 1052 cm⁻¹. The absence of these characteristic peaks confirms the binding of dye molecule onto adsorbent moieties.

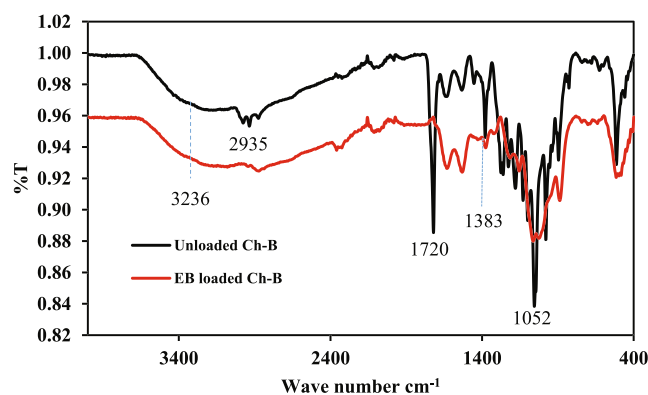


FIGURE 3 The FT-IR spectra of Ch-B composite of unloaded and loaded EB dye

3.1.2 | SEM-EDX analyses

SEM technique has been applied to analyze the surface morphology of **Ch-B** adsorbent (Figure 4). In Figure 4, image A is of unloaded **Ch-B** adsorbent, which shows clear and smooth surface while image B is of **EB** dye loaded **Ch-B** adsorbent which is rough and amorphous. The roughness confirms the loading if **EB** dye onto **Ch-B** adsorbent.

EDX spectra indicated the existence of B, C, N, and O elements before adsorption (Figure 4C). After adsorption, the appearance of I was seen to increase (Figure 4D). Taken together, the analytical and visual data produced concordant results.

3.2 | Effect of initial pH on EB dye adsorption

During the batch study, it has been observed that the adsorption percentage was increased by increasing the pH from 2 to 8 (Figure 5). This adsorption behavior of **EB** dye onto **Ch-B** adsorbent can be explained on the basis of ionic interaction between the adsorbent surface moieties and **EB** dye. The adsorbent surface is composed of oxygen and nitrogen moieties which bears negative charge on it. In acidic media the adsorbent surface was

saturate with positive charge that attracts the negative part of dye molecule.

3.3 | Effect of Ch-B adsorbent dosage

Adsorbent dosage is very important parameters because it describes the efficiency as well as capacity of material.

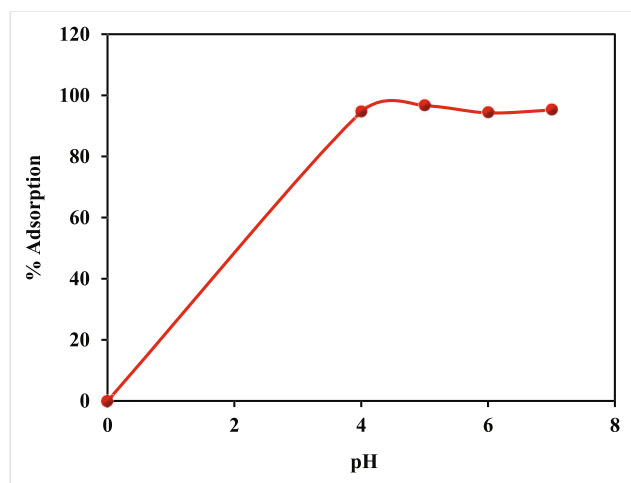


FIGURE 5 Effect of pH on adsorption of **EB** dye using **Ch-B** adsorbent

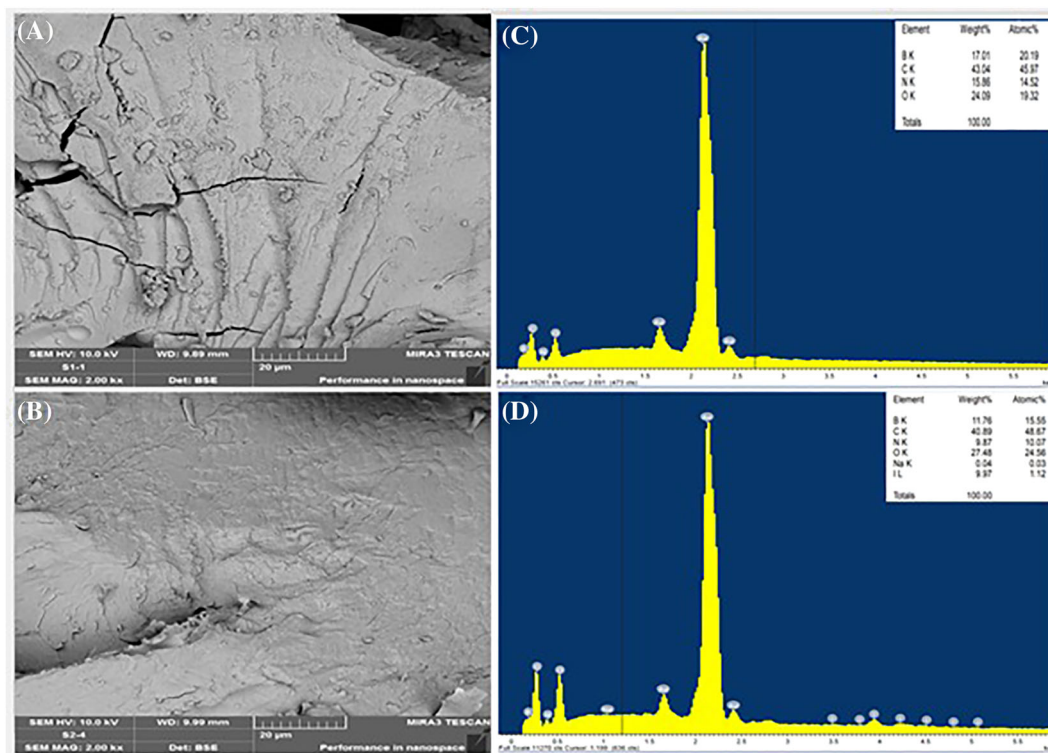


FIGURE 4 SEM images of **EB** adsorption before (A) and after (B) and EDX spectrums of **EB** adsorption before (C) and after (D)

Herein, different doses of Ch-B adsorbents were optimized ranges from 0.025 to 0.25 g·L⁻¹ (Figure 6). During the experiments, it has been observed that the adsorption percentage was increased with increasing adsorbent dose from 0.025 to 0.05, and then it becomes constant due to complete saturation of adsorbent surface and adsorption capacity is completely filled by EB dye molecule.

3.4 | Isotherm models

Equilibrium data were subjected to the Langmuir, Freundlich, and Dubinin-Radushkevich (D-R) isotherm models to understand the adsorption nature of EB dye onto Ch-B adsorbent. The Langmuir, Freundlich, and D-R isotherm models can be calculated using the following Equations (8)–(10), respectively.

$$\left(\frac{C_e}{C_{ads}}\right) = \left(\frac{1}{Qb}\right) + \left(\frac{C_e}{Q}\right) \quad (8)$$

$$\log C_{ads} = \log A + \left(\frac{1}{n}\right) \log C_e \quad (9)$$

$$\ln C_{ads} = \ln X_m - \beta e^2 \quad (10)$$

where C_e and C_{ads} are equilibrium and adsorbed concentrations and Q (mol·g⁻¹) is the Langmuir adsorption capacity. A is Freundlich constant shows the relative adsorption capacity of the adsorbent (mol·g⁻¹) while the constant $1/n$ indicates the intensity of the adsorption.

Langmuir isotherm model is used to describe the equilibrium adsorption isotherms of homogeneous system. Thus, the Langmuir model has been applied following the equation (4) on equilibrium data by plotting the graph in between C_e/C_{ads} versus C_e (Figure 7). From the

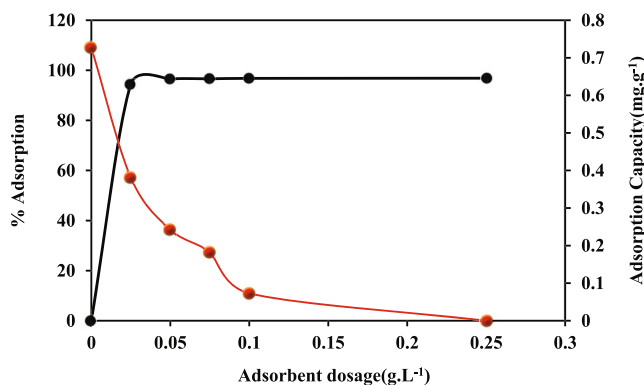


FIGURE 6 Effect of adsorbent dosage on EB dye adsorption from water

slope and intercept, the constant values have been calculated (Table 1). The Freundlich model describes the heterogeneous and reversible adsorption equilibriums. The

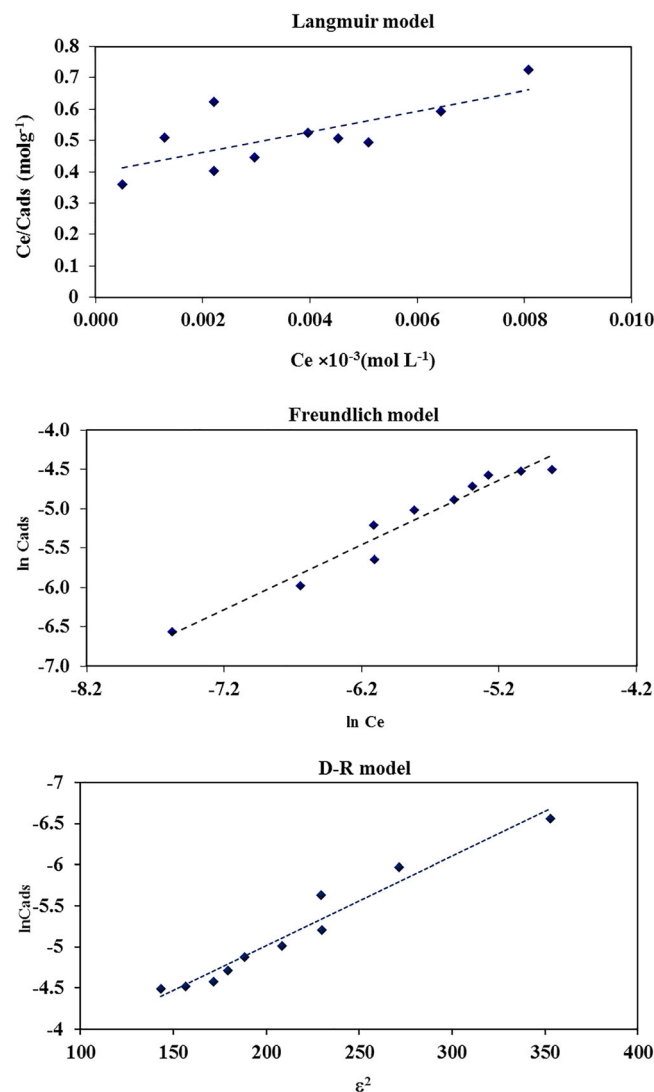


FIGURE 7 The linear graphs of Langmuir, Freundlich, and D-R isotherm models for the adsorption of EB dye onto Ch-B adsorbent

TABLE 1 Adsorption isotherm model parameters

Parameters	Langmuir	Freundlich	D-R
Q (mol·g ⁻¹)	0.032	–	–
b (L·mol ⁻¹)	83	–	–
R_L	0.65–0.99	–	–
R^2	0.5304	0.9559	0.9147
A (mol·g ⁻¹)	–	36.58	–
X_m (mol·g ⁻¹)	–	–	0.058
$1/n$	–	0.8233	–
E (KJ/mol)	–	–	8.19

equilibrium data have been analyzed using Equation (5), and graph has been plotted between $\ln C_{ads}$ versus $\ln C_e$ (Figure 7). From the slope and intercept, the constant values were calculated (Table 1). The D-R model is used to differentiate between physical and chemical adsorption mechanisms. The graph has been plotted between (ϵ) versus $\ln C_{ads}$ ($\text{mol}\cdot\text{g}^{-1}$) (Figure 7); from the slope and intercept, the constant values were calculated (Table 1). According to the results given in Table 1, the EB dye has good fitting with Freundlich model ($R^2 = 0.90$) with a favorable $1/n$ value (0.823), suggesting the physical interaction between dye and adsorbent surface. The values of D-R model ($X_m = 0.058 \text{ mol}\cdot\text{g}^{-1}$, $E = 8.19 \text{ KJ}\cdot\text{mol}^{-1}$) suggested that the adsorption of EB dye is physical in nature.

3.5 | Thermodynamic study

The thermodynamic study has been performed, and parameters such as (ΔH) change in enthalpy, (ΔS) entropy, and (ΔG) Gibbs free energy were calculated using equilibrium data at various temperature (i.e., 298, 303, and 308 K) on the adsorption of the EB dye. The thermodynamic parameters (ΔH , ΔS , and ΔH) (Table 2) have been calculated from the slope and intercept of the linear plot of $\ln k_c$ versus $1/T$ (Figure 8) using the following equations (11) and (12).

$$\ln k_c = \frac{-\Delta H}{RT} + \frac{\Delta S}{R} \quad (11)$$

$$\Delta G = -RT \ln k_c \quad (12)$$

where k_c is equilibrium constant. The thermodynamic constant values (Table 2) demonstrate that the adsorption of EB dye onto Ch-B adsorbent is spontaneous due to the negative values of (ΔG) and endothermic due to positive value of (ΔH). Moreover, the positive value of ΔS indicates that randomness is increased at adsorbent surface during equilibrium between dye and adsorbent molecules.

3.6 | Kinetic study

In kinetic study, the rate of adsorption of EB dye onto Ch-B adsorbent was determined by applying the pseudo-

first-order and pseudo-second-order models. Thus, the graph has been plotted between $\ln(q_e - q_t)$ versus t time using Equation (13) (Figure 9), and constant parameters were obtained from linear plot (Table 3).

$$\ln(q_e - q_t) = \ln q_e - k_1 t \quad (13)$$

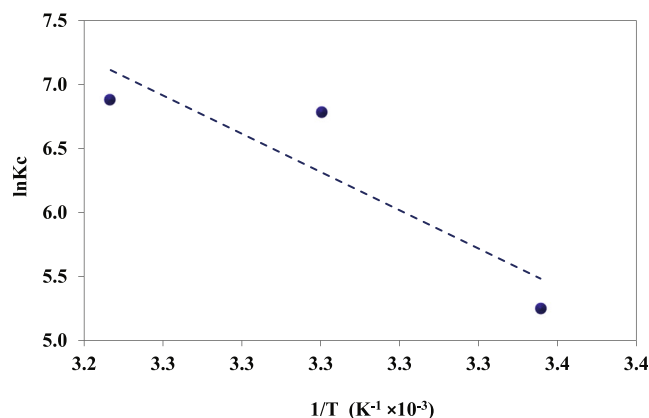


FIGURE 8 Effect of the temperature on the adsorption of EB dye using Ch-B adsorbent

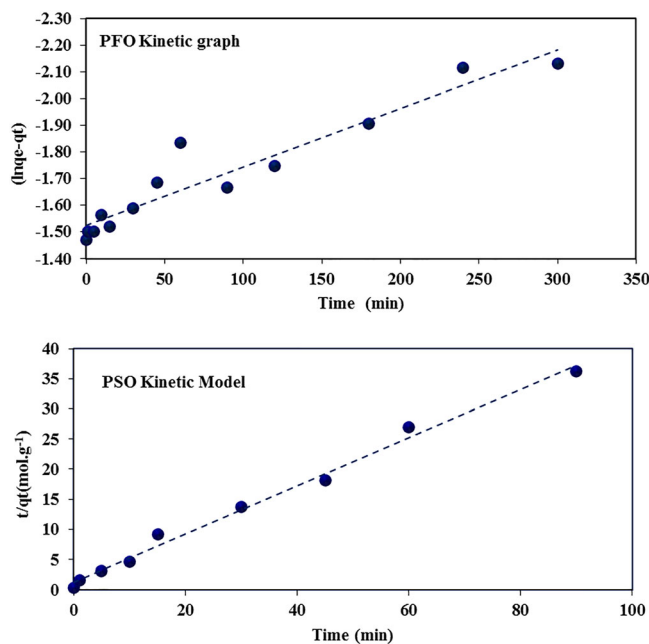


FIGURE 9 Pseudo first- and pseudo second-order kinetic graph for the adsorption of EB dye

ΔH (KJ/mol)	ΔS (KJ/mol)	ΔG (KJ/mol)		
0.124	0.462	298 K	303 K	308 K
		-13.01	-17.06	-17.60
		$\ln K_c = 5.3$	$\ln K_c = 6.8$	$\ln K_c = 6.9$

TABLE 2 Thermodynamic parameters for the adsorption of EB dye using Ch-B adsorbent

TABLE 3 Kinetic parameters for adsorption of EB dye

	Pseudo first order			Pseudo second order		
	K_1 (min ⁻¹)	q_e (mol/g)	R^2	K_2 (min ⁻¹)	q_e (g/mol·min ⁻¹)	R^2
Erythrosine B	0.0023	0.22	0.912	0.12	6.27	0.991

TABLE 4 Calculated electronic characteristics of isolated molecules

Name	Molecule formula	Dipole moment (Debye)	HOMO (eV)	LUMO (eV)	χ (eV)	η (eV)	ω (eV)
Boric acid	BH ₃ O ₃	0.011	-7.238	0.117	3.560	7.355	0.861
Chitosan	C ₂₄ N ₄ H ₄₆ O ₁₇	4.166	-5.086	-0.190	2.638	4.895	0.710
Erythrosine	C ₂₀ H ₈ O ₅ I ₄	5.482	-5.682	-2.724	4.203	2.958	2.986

TABLE 5 Calculated energy and electronic characteristics of chitosan/boric acid complex

Name	Molecule formula	Dipole moment (Debye)	HOMO (eV)	LUMO (eV)	χ (eV)	η (eV)	ω (eV)	E_b , eV
Chitosan/boric acid	C ₂₄ N ₄ H ₄₆ O ₁₇ /4BH ₃ O ₃	3.410	-5.208	-0.691	2.949	4.517	0.962	3.76

TABLE 6 Calculated energy and electronic characteristics of erythrosine adsorbed on the chitosan/boric acid complex

Name	Molecule formula	Dipole moment (Debye)	HOMO (eV)	LUMO (eV)	χ (eV)	η (eV)	ω (eV)	E_b , eV
Erythrosine-chitosan/ boric acid	C ₂₀ H ₈ O ₅ I ₄ -C ₂₄ N ₄ H ₄₆ O ₁₇ /4BH ₃ O ₃	7.378	-5.663	-2.852	4.257	2.811	3.224	1.75

where q_t is the adsorbed amount of EB dye (mol·g⁻¹) and (k_1 /min) is the first-order rate constant.

The pseudo second-order kinetic model has been applied using the equation (14):

$$\frac{t}{q_t} = \left(\frac{t}{k_2 q_e^2} \right) + \left(\frac{1}{q_e} \right) \quad (14)$$

where K_2 is rate constant and q_e is equilibrium concentration. Equilibrium data have been subjected by plotting the graph between t/q_t versus t in Figure 9, which demonstrate a good linear relationship while the values of q_e and K_2 have been obtained from the slope and intercept of the plot mentioned in Table 3.

3.7 | Results of DFT calculations

In such projects, the highlighting of the power and the nature of the interactions between chemical systems studied is quite important. For this aim, conceptual

density functional theoretical parameters and some important electronic structure principles like maximum hardness^[35] and minimum polarizability principles^[36] are widely preferred. In Table 4, calculated quantum chemical parameters regarding to the isolated forms of boric acid, chitosan, and erythrosine structures are given. Table 5 presents the calculated energy and electronic characteristics of chitosan/boric acid complex. The binding energy E_b is defined as $E_b = E(\text{Chitosan}) + E(\text{Boric acid}) - E(\text{Chitosan/Boric Acid})$. The values of E_b as well as electronic characteristics are presented in Table 5. Table 6 includes calculated binding energy and electronic characteristics of Erythrosine adsorbed on the chitosan/boric acid complex. The binding energy E_b is defined as $E_b = E(\text{Erythrosine}) + E(\text{Chitosan/Boric Acid}) - E(\text{Erythrosine-Chitosan/Boric Acid})$. The values of E_b as well as electronic characteristics are presented in Table 6.

Figures 10–14 include optimized structures and HOMO and LUMO images and studied chemical systems and the complex systems forming as a result of the interaction between these systems. Chemical hardness^[37,38] is

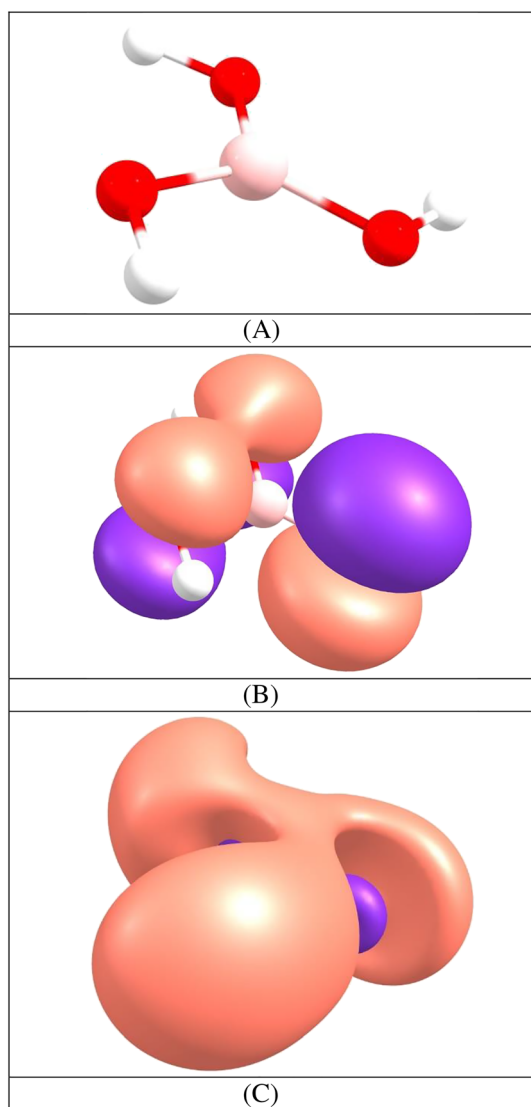


FIGURE 10 Boric acid: atomic structure (A), HOMO (B), and LUMO (C)

presented as the resistance against the polarization of electron cloud of atomic, ionic, and molecular systems. According to hard and soft acid-base principle^[39] introduced based on chemical hardness concept by Pearson, “hard acids prefer to coordinate to hard bases and soft acids prefer to coordinate to soft bases.” It is important to note that HSAB principle found many applications in the literature. For instance, toxic effect of heavy metal ions can be explained in the light of HSAB principle because heavy metal ions are soft acids, and they interact strongly with amino acids containing sulfur atoms in their structure, such as cysteine and methionine. Additionally, HSAB principle is widely considered in the design and synthesis of ionic liquids exhibiting great corrosion inhibition performances. The products of the substitution

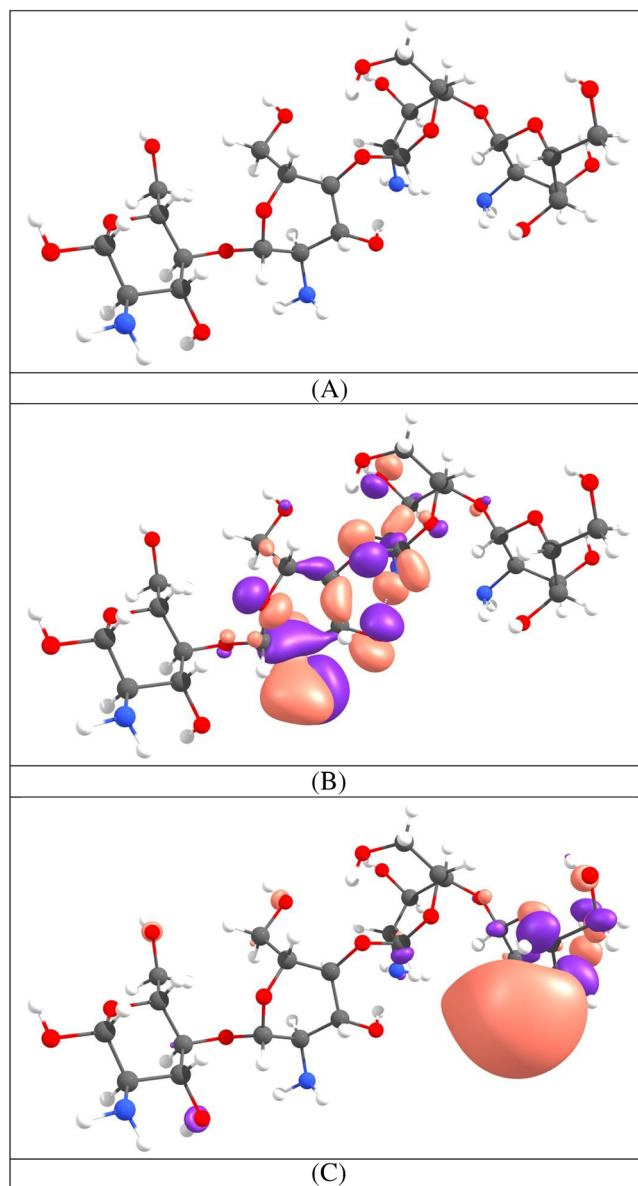


FIGURE 11 Chitosan: atomic structure (A), HOMO (B), and LUMO (C)

reactions and double exchange reactions can be predicted within the framework of HSAB Principle. Recently, some authors^[40,41] noted that HSAB principle is useful for the explanation of biochemical interactions.

Maximum hardness principle states that hard chemical systems are more stable compared with soft ones. It can be seen from the results given in Table 4 that chitosan and boric acids systems are very hard. It is not difficult to say that the interaction between chitosan and boric acid should be powerful. This can be easily predicted through hard and soft acid-base principle. Binding energy calculated for the interaction between chitosan and boric acid is 3.76 eV. This value is in good agreement

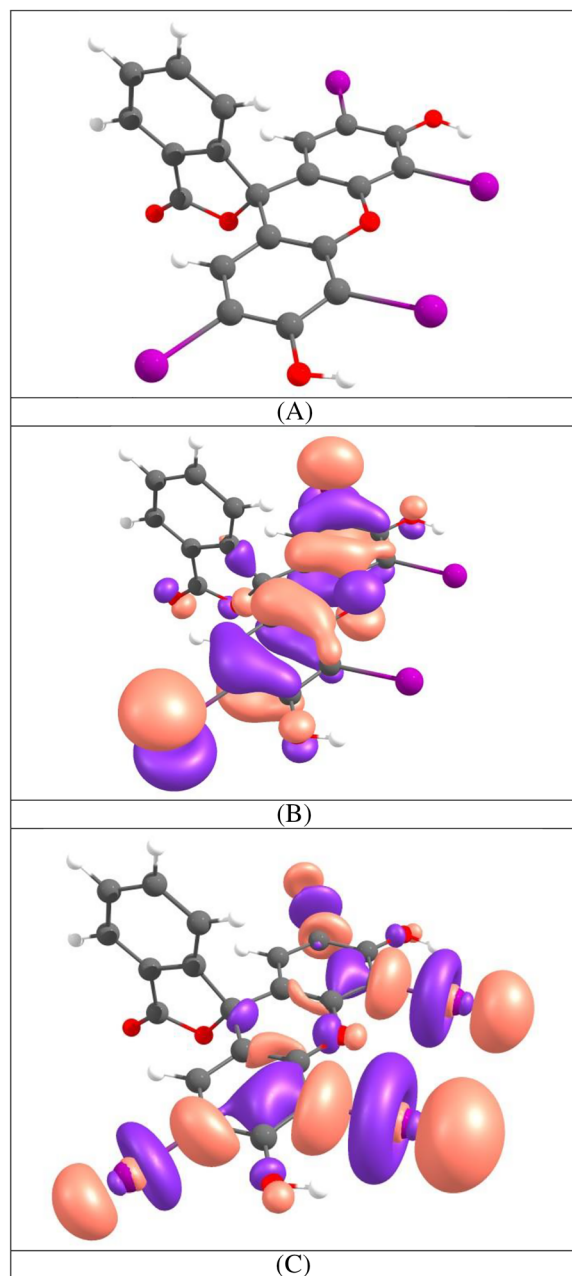


FIGURE 12 Erythrosine: atomic structure (A), HOMO (B), and LUMO (C)

with the predictions made via HSAB principle. Binding energy value calculated for the interaction with chitosan–boric acid complex of erythrosine is 1.76 eV. This value shows that chitosan–boric acid system acts as an effective adsorbent for the removal of Erythrosine from wastewater. Theoretical findings support the experimental observations.

Recently, Nascimento et al.^[42] designed a nanoadsorbent from Amazon bauxite tailings for the removal of

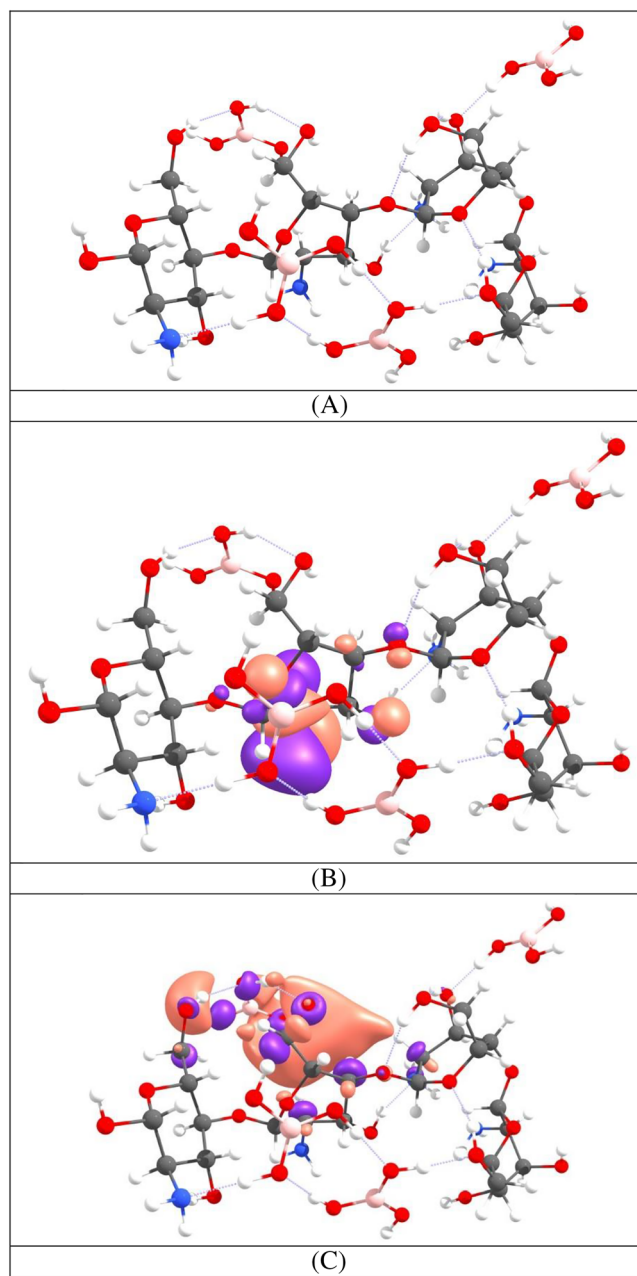


FIGURE 13 Chitosan/boric acid complex: atomic structure (A), HOMO (B), and LUMO (C)

erythrosine B dye. Then, Fazlzadeh et al.^[43] published a paper on green synthesis of zinc oxide nanoparticles loaded on activated carbon prepared from walnut peel extract for the removal of eosin Y and erythrosine B dyes from aqueous solution. It should be noted that the chitosan boric acid composite designed by us exhibits high performance like the materials introduced by Nascimento and Fazlzadeh for the removal of erythrosine B dye from wastewater.

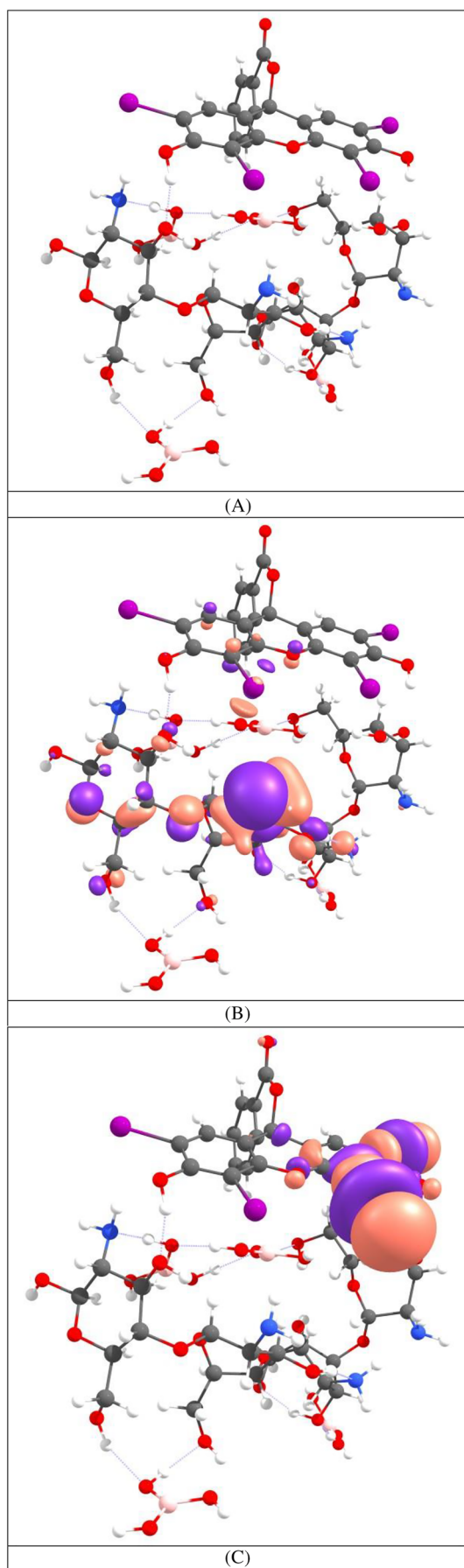


FIGURE 14 Erythrosine adsorption on the chitosan/boric acid complex: atomic structure (A), HOMO (B), and LUMO (C)

4 | CONCLUSION

A new composite material including chitosan and boric acid with the help of epichlorohydrin and tripolyphosphate cross linkers. The reliability of the synthesis made was proved via FTIR spectra and SEM images. The performance of this composite material to remove the Erythrosine from waste water was analyzed using some experimental and theoretical tools. The experimental data obtained are in good agreement with Freundlich adsorption model. Both experimental and theoretical results proved that new designed chitosan–boric acid composite is an effective adsorbent for the removal of the Erythrosine from waste water. Interaction mechanisms proposed and binding energies calculated for the studied chemical systems showed that our results support the HSAB principle. Experimental observations proved that adsorption process is exothermic and spontaneous.

CONFLICT OF INTEREST

All authors declared no conflicts of interest.

DATA AVAILABILITY STATEMENT

Data can be available.

ORCID

Savaş Kaya  <https://orcid.org/0000-0002-0765-9751>

REFERENCES

- [1] Z. Badani, H. Ait-Amar, A. Si-Salah, M. Brik, W. Fuchs, *Desalination* **2005**, *185*, 411. <https://doi.org/10.1016/j.desal.2005.03.088>
- [2] J. Guo, S. Chen, L. Liu, B. Li, P. Yang, L. Zhang, Y. Feng, *J. Colloid Interface Sci.* **2012**, *382*, 61. <https://doi.org/10.1016/j.jcis.2012.05.044>
- [3] A. H. Jawad, S. S. A. Norrahma, B. H. Hameed, K. Ismail, *Int. J. Biol. Macromol.* **2019**, *135*, 569.
- [4] A. H. Jawad, M. A. Nawi, M. H. Mohamed, L. D. Wilson, *J. Polym. Environ.* **2017**, *25*, 828. <https://doi.org/10.1016/j.ijbiomac.2019.05.127>
- [5] A. H. Jawad, N. H. Mamat, B. H. Hameed, K. Ismail, *J. Environ. Chem. Eng.* **2019**, *7*, 102965. <https://doi.org/10.1016/j.jece.2019.102965>
- [6] S. Hydari, H. Sharifard, M. Nabavinia, M. R. Parvizi, *Chem. Eng. J.* **2012**, *193*, 276. <https://doi.org/10.1016/j.cej.2012.04.057>
- [7] A. S. Abdulhameed, A. T. Mohammad, A. H. Jawad, *Desalin Water Treat.* **2019**, *164*, 346. <https://doi.org/10.5004/dwt.2019.24384>
- [8] A. S. Abdulhameed, A. H. Jawad, A. T. Mohammad, *Bioresour. Technol.* **2019**, *293*, 122071. <https://doi.org/10.1016/j.biortech.2019.122071>

- [9] L. Zhang, L. Sellaoui, D. Franco, G. L. Dotto, A. Bajahzar, H. Belmabrouk, Z. Li, *Chem. Eng. J.* **2020**, 382, 122952. <https://doi.org/10.1016/j.cej.2019.122952>
- [10] Z. Li, L. Sellaoui, G. L. Dotto, A. B. Lamine, A. Bonilla-Petriciolet, H. Hanafy, A. Erto, *J. Mol. Liq.* **2019**, 285, 165. <https://doi.org/10.1016/j.molliq.2019.04.091>
- [11] A. H. Jawad, A. S. Abdulhameed, M. S. Mastuli, *J. Polym. Environ.* **2020**, 28, 1095. <https://doi.org/10.1007/s10924-020-01671-5>
- [12] M. Vakili, S. Deng, T. Li, W. Wang, W. Wang, G. Yu, *Chem. Eng. J.* **2018**, 347, 782. <https://doi.org/10.1016/j.cej.2018.04.181>
- [13] I. Tahira, Z. Aslam, A. Abbas, M. Monim-ul-Mehboob, S. Ali, A. Asghar, *Int. J. Biol. Macromol.* **2019**, 136, 1209. <https://doi.org/10.1016/j.ijbiomac.2019.06.173>
- [14] M. E. Mahmoud, A. M. El-Ghanam, R. H. A. Mohamed, S. R. Saad, *Mater. Sci. Eng. C* **2020**, 108, 110199. <https://doi.org/10.1016/j.msec.2019.110199>
- [15] A. S. Abdulhameed, A. T. Mohammad, A. H. Jawad, *J. Clean. Prod.* **2019**, 232, 43. <https://doi.org/10.1016/j.jclepro.2019.05.291>
- [16] A. A. Alhwaige, H. Ishida, S. Qutubuddin, *Carbohydr. Polym.* **2019**, 209, 122. <https://doi.org/10.1016/j.carbpol.2019.01.016>
- [17] A. H. Jawad, A. S. Abdulhameed, E. Kashi, Z. A. AlOthman, M. R. Khan, *J. Polym. Environ.* **2021**, 30, 164. <https://doi.org/10.1016/j.arabjc.2022.103757>
- [18] Y. Anwar, *Int. J. Biol. Macromol.* **2018**, 111, 1140. <https://doi.org/10.1016/j.ijbiomac.2018.01.096>
- [19] T. Kameda, R. Honda, S. Kumagai, Y. Saito, T. Yoshioka, *Mater. Chem. Phys.* **2019**, 236, 121784. <https://doi.org/10.1016/j.matchemphys.2019.121784>
- [20] Q. Liu, B. Yang, L. Zhang, R. Huang, *Int. J. Biol. Macromol.* **2015**, 72, 1129. <https://doi.org/10.1016/j.ijbiomac.2014.10.008>
- [21] H. J. Kumari, P. Krishnamoorthy, T. Arumugam, S. Radhakrishnan, D. Vasudevan, *Int. J. Biol. Macromol.* **2017**, 96, 324.
- [22] W. S. W. Ngah, L. C. Teong, C. S. Wong, M. A. K. M. Hanafiah, *J. Appl. Polym. Sci.* **2012**, 125, 2417. <https://doi.org/10.1002/app.36503>
- [23] C. Lee, W. Yang, R. G. Parr, *Phys. Rev. B* **1988**, 37, 785. <https://doi.org/10.1103/PhysRevB.37.785>
- [24] A. D. Becke, *J. Chem. Phys.* **1993**, 98, 5648.
- [25] M. M. Francl, W. J. Pietro, W. J. Hehre, J. S. Binkley, M. S. Gordon, *Chem. Phys.* **1982**, 77, 3654. <https://doi.org/10.1063/1.444267>
- [26] I. S. Ufimtsev, T. J. Martínez, *J. Chem. Theo. Comp.* **2009**, 5, 2619. <https://doi.org/10.1021/ct9003004>
- [27] A. V. Titov, I. S. Ufimtsev, N. Luehr, T. J. Martínez, *J. Chem. Theo. Comp.* **2013**, 9, 213. <https://doi.org/10.1021/ct300321a>
- [28] J. Kästner, J. M. Carr, T. W. Keal, W. Thiel, A. Wander, P. Sherwood, *J. Phys. Chem. A* **2009**, 113, 11856. <https://doi.org/10.1021/jp9028968>
- [29] T. P. M. Goumans, C. R. A. Catlow, W. A. Brown, J. Kästner, P. Sherwood, *Phys. Chem. Chem. Phys.* **2009**, 11, 5431. <https://doi.org/10.1039/B816905E>
- [30] L. P. Wang, C. Song, *J. Chem. Phys.* **2016**, 144, 214108. <https://doi.org/10.1063/1.4952956>
- [31] S. Grimme, J. Antony, S. Ehrlich, H. Krieg, *J. Chem. Phys.* **2010**, 132, 154104. <https://doi.org/10.1063/1.3382344>
- [32] *Conceptual density functional theory and its application in the chemical domain* (Eds: N. Islam, S. Kaya), CRC Press **2018**.
- [33] I. B. Obot, S. Kaya, C. Kaya, B. Tüzün, *Phys. E: Low-Dimens. Syst. Nanostructures.* **2016**, 80, 82. <https://doi.org/10.1016/j.physe.2016.01.024>
- [34] T. Koopmans, *Phys. Ther.* **1934**, 1, 104. [https://doi.org/10.1016/S0031-8914\(34\)90011-2](https://doi.org/10.1016/S0031-8914(34)90011-2)
- [35] S. Kaya, C. Kaya, *Inorg. Chem.* **2015**, 54(17), 8207. <https://doi.org/10.1021/acs.inorgchem.5b00383>
- [36] S. Kaya, C. Kaya, N. Islam, *Phys. B: Condens. Matter.* **2016**, 485, 60. <https://doi.org/10.1016/j.physb.2016.01.010>
- [37] S. Kaya, C. Kaya, *Mol. Phys.* **2015**, 113(11), 1311. <https://doi.org/10.1080/00268976.2014.991771>
- [38] S. Kaya, C. Kaya, *Comput. Theor. Chem.* **2015**, 1060, 66. <https://doi.org/10.1016/j.comptc.2015.03.004>
- [39] R. G. Pearson, *J. Am. Chem. Soc.* **1963**, 85(22), 3533.
- [40] T. L. Ho, H. C. Ho, L. D. Hamilton, *Chem. Biol. Interact.* **1978**, 23(1), 65.
- [41] R. M. LoPachin, T. Gavin, A. DeCaprio, D. S. Barber, *Chem. Res. Toxicol.* **2012**, 25(2), 239.
- [42] R. S. Nascimento, J. A. M. Corrêa, B. A. M. Figueira, P. A. Pinheiro, J. H. Silva, P. T. C. Freire, S. Quaranta, *Appl. Clay Sci.* **2022**, 222, 106482.
- [43] Y. Rashtbari, S. Afshin, A. Hamzezhadeh, A. Gholizadeh, F. J. Ansari, Y. Poureshgh, M. Fazlzadeh, *Environ. Sci. Pollut. Res.* **2022**, 29(4), 5194.

How to cite this article: H. F. Çetinkaya, M. S. Cebeci, S. Kaya, N. S. Jalbani, M. M. Maslov, R. Marzouki, *J Phys Org Chem* **2023**, 36(12), e4400. <https://doi.org/10.1002/poc.4400>